

Microwave Radiometric Technique to Retrieve Vapor, Liquid and Ice, Part I—Development of a Neural Network-Based Inversion Method

Li Li, J. Vivekanandan, C. H. Chan, and Leung Tsang, *Fellow, IEEE*

Abstract—With the advent of the microwave radiometer, passive remote sensing of clouds and precipitation has become an indispensable tool in a variety of meteorological and oceanographical applications. There is wide interest in the quantitative retrieval of water vapor, cloud liquid, and ice using brightness temperature observations in scientific studies such as earth's radiation budget and microphysical processes of winter and summer clouds. Emission and scattering characteristics of hydrometeors depend on the frequency of observation. Thus, a multifrequency radiometer has the capability of profiling cloud microphysics. Sensitivities of vapor, liquid, and ice with respect to 20.6, 31.65 and 90 GHz brightness temperatures are studied. For the model studies, the atmosphere is characterized by vapor density and temperature profiles and layers of liquid and ice components. A parameterized radiative transfer model is used to quantify radiation emanating from the atmosphere. It is shown that downwelling scattering of radiation by an ice layer results in enhancement at 90 GHz brightness temperature. Once absorptive components such as vapor and liquid are estimated accurately, then it is shown that the ice water path can be retrieved using ground-based three-channel radiometer observations. In this paper we developed two- and three-channel neural network-based inversion models. Success of a neural network-based approach is demonstrated using a simulated time series of vapor, liquid, and ice. Performance of the standard explicit inversion model is compared with an iterative inversion model. In Part II of this paper, actual radiometer, and radar field measurements are utilized to show practical applicability of the inverse models.

I. INTRODUCTION

GROUND-BASED dual-channel radiometers have been used successfully for more than 20 years to monitor vapor and cloud water [1]–[4]. Radiometric measurements of total precipitable water vapor column are about the same as, or better than, those of radiosondes [3]. Retrievals from ground-based radiometers are also used as a validation for satellite sensors. Unlike radiosondes, radiometers provide measurements unattendedly and continuously. Westwater [1] and Staelin [5]

Manuscript received October 27, 1994; revised March 4, 1996. This work is supported by the National Science Foundation through an interagency agreement in response to requirements and funding by the Federal Aviation Administration's Aviation weather development program. The views expressed are those of the authors and do not necessarily represent the official policy or position of the U.S. Government.

L. Li is with the National Center for Atmospheric Research, Boulder, CO 80307 USA. He is also with the Department of Electrical Engineering, University of Washington, Seattle, WA 98195 USA.

J. Vivekanandan is with the National Center for Atmospheric Research, Boulder, CO 80307 USA.

C. H. Chan and L. Tsang are with the Department of Electrical Engineering, University of Washington, Seattle, WA 98195 USA.

Publisher Item Identifier S 0196-2892(97)00366-5.

investigated the microwave spectrum of the atmosphere and its sensitivities to atmospheric components such as vapor, liquid, air temperature, and gaseous absorption which provided the basis for most of the radiometric retrieval methods. In their investigations, statistical techniques were more or less utilized to deal with the variability of vapor and liquid components of atmospheric media both in time and space. Based on this, simple physical and linear/nonlinear statistical algorithms were developed for ground-based radiometers to quantitatively retrieve water vapor and liquid cloud information under non-precipitation conditions [6]. Simple physical methods which oversimplify the real problems are less accurate than statistical ones, but statistical methods offer no insights to the physical processes. Most of the existing algorithms break down if Mie scattering due to ice and water drops is present because the earlier models are based on absorption. For example, retrieval accuracies are marginal for cloud liquid much in excess of 3 mm [3], [7], [8].

Despite the successes of statistical models, physical models are highly desirable. Retrieval techniques based on physical models are considered nonunique in nature. However, with the advent of remote sensing techniques, auxiliary measurements, including measurements other than brightness temperatures, can be incorporated to improve the confidence in remote sensing methods and to reduce ambiguities in the estimation of atmospheric components. Examples of auxiliary measurements are polarimetric and multifrequency radiometer data, radar data, and radio acoustic sounding system (RASS) data [9]–[11]. A comprehensive physical forward model which includes spatial distribution of atmospheric variables is crucial for quantitative investigation of sensitivities of each of the microphysical quantities such as vapor, cloud water, and ice. Thus, the forward model plays a key role in understanding microphysics and retrieval of the same.

The parameterization approach is useful for physical models of ill-posed problems as in the case of microwave radiometry [12]. It describes the state of the atmosphere using a limited number of unknowns and lessens the ambiguities in inversion; it also provides a methodology for extracting information from radiometer measurements. To date, the majority of algorithms is based on more or less oversimplified forward (radiative transfer) models, which represent the relationship between brightness temperatures and microphysical quantities. Such an algorithm retrieves microphysical quantities using a set of algebraic expressions. In this paper, we first developed

a parametric radiative transfer model as a general forward model, which is tested against rigorous numerical models. The parametric model is used to carry out a sensitivity study between brightness temperatures and atmospheric components. Based on the sensitivity study, several different inverse models are implemented using artificial neural networks (ANN). The parametric model deals with vertical distribution of absorption and scattering phenomenon of atmospheric components [12], [13].

The paper is organized as follows. Section II outlines the theoretical description of a parametric forward radiative transfer model. Temperature and vapor density profiles and the corresponding radiative properties of atmospheric gases are parameterized. A millimeter-wave propagation model [18] is used to obtain radiative properties of gases. Subsequently, a complete radiative transfer model is developed by combining emission due to atmospheric gases and cloud liquid water and also scattering due to the ice layer. The parametric radiative transfer model results are compared with the rigorous radiative transfer computations [21] and actual brightness temperature measurements in Section III. Also sensitivities of 20.6, 31.65, and 90 GHz brightness temperature to vapor, cloud water, and ice are discussed. Based on the sensitivity studies, a procedure to construct a neural network-based inverse model to retrieve vapor, liquid and ice is outlined in Section IV. Both explicit inversion and iterative inversion neural networks are considered. Section V shows the performances of explicit inversion and iterative inversion neural network models. It is shown that an iterative inversion model is better than the explicit inversion model. Finally, the paper ends with discussion and conclusions in Section VI.

II. MODEL DEVELOPMENT

The main objective of passive microwave remote sensing of the atmosphere is to extract atmospheric quantities using appropriate retrieval techniques. In principle, the development of a retrieval technique consists of several phases. In this research, we used the following procedure. The first phase is to parameterize atmospheric components. Parameterization leads to simplification of cumbersome vertical profile descriptions of temperature and vapor density. The second phase is to study the response of brightness temperature to changes in micro-physical quantities. This is known as the forward radiative transfer problem. Finally, an appropriate retrieval (or inverse) model is developed based on simulation results.

The atmosphere is characterized by high degrees of variability in time and space. A large number of unknowns are generally needed to describe the states of an atmosphere. With a limited number of measurements, a complete characterization of atmosphere is an ill-posed problem and no unique solution can be obtained. This is the main reason why statistical methods are widely used in radiometry models. On the other hand, it is neither necessary, nor possible, to take enough measurements and determine the state of the atmosphere in much detail. Instead, the questions that should always be asked first are: What is the best way to parameterize the problem at hand, and what kind of information is retrievable from a

given set of measurements? One of the practical solutions to these questions is a parametric radiative transfer model, which can offer a realistic description and detailed sensitivity studies of the remote sensing problem. The major advantage of the parameterized radiative transfer model is that a detailed description of temperature and vapor density (ρ_v) is specified by a finite number of distinctive parameters. As we know, a statistical retrieval algorithm is based on average states of atmospheric profile, and is of little help in the presence of precipitation. On the other hand, a physical model does not depend on geophysical location, but could have larger inherent biases if model results are not compared with actual measurement. The procedure for the construction of a neural network based inverse model consists of the following steps:

- 1) develop a parameterized forward-model;
- 2) conduct sensitivity studies using the parameterized model to identify the primary atmospheric components which are the most sensitive;
- 3) generate three-channel brightness temperatures over the range of the atmospheric components;
- 4) construct neural network based inverse models using the combinations of brightness temperature.

III. MODEL ATMOSPHERE

Supercooled liquid water (SLW) is known to cause aircraft icing, which continues to be one of the primary causes of aviation accidents, especially in winter weather situations [14]. A parametric radiative transfer model developed here focuses on the detection and estimation of supercooled water, vapor, and ice in winter clouds. The size of the SLW droplet ranges from tens to hundreds of micrometers. Temperatures for SLW can be as low as -20°C . Growth and formation of snow or other ice particles in a cloud quickly depletes supercooled cloud droplets. Thus the liquid water content (LWC) is very small in the presence of ice crystals [14]. In-situ measurements by research aircraft show that the LWC usually increases slowly with height to a maximum value, then decreases quickly near cloud top [10]. This kind of liquid water profile information has been assimilated into liquid water and water vapor profiling using combined remote sensors. However, in this paper, we use uniform profiles for both liquid and ice clouds for the following two reasons. First, our main focus is on the improvements of liquid and ice column retrieval, not the liquid water profiling. Second, without auxiliary measurements from other remote sensors like radar and RASS it is difficult to obtain vertical profiles. Also, the effects of a detailed liquid water profile are less significant in the brightness temperature computations, which can be seen from sensitivity studies in a later section of this paper.

The drop size distribution of supercooled water drops is described by exponential or Gamma function. However, scattering due to liquid drops with sizes less than 0.1 mm is too small. Absorption or emission of water drops is proportional to mass per unit volume. In contrast to supercooled liquid water droplets, ice crystals have much larger sizes. Their shapes, bulk density, and size distributions have profound impacts on passive remote sensing. Since most of the ground-

based radiometers do not measure polarimetric radiation from atmosphere, ice particle shapes are approximated as equivalent spheres. Their size distribution is assumed as modified Gamma size distributions [15]

$$n(r) = ar^\alpha \exp(-br^\gamma) \quad (1)$$

where r is the radius of particles, α and γ are empirical constants, $n(r)$ is the number of particles per unit volume per unit radius. The value of parameters α and γ are set to two and one, respectively.

The parameters 'a' and 'b' are related to mode radius r_c , bulk density ρ and ice water content (IWC) as

$$b = \frac{2}{r_c} \quad (2)$$

and

$$a = \frac{b^6}{160\pi\rho} \text{IWC}. \quad (3)$$

Radiosondes measure vertical profiles of relative humidity (or vapor density), pressure, temperature (T) and dew point (T_d) in the lower atmosphere. Fig. 1 shows an example of a radiosonde measurement taken on 2 March 1991 at Platteville, Colorado. Derived quantities such as mixing ratio (mr) and vapor density are also shown. The air temperature decreased smoothly with height except that there was a temperature inversion near the ground. The temperature profile can be approximated by a linear relationship

$$T(z) = T_A - \Gamma z \quad (4)$$

where T_A and Γ are effective near-ground temperature and lapse rate, respectively. It should be noted that T_A and Γ are effective variables and are not necessarily equal to the actual near surface temperature and mean lapse rate, respectively [12]. For the forward problem, T_A and Γ can be directly calculated from radiosonde observations [16]

$$T_A = 4\bar{T} - 6T_\sigma \quad (5)$$

and

$$\Gamma = \frac{6}{H}[\bar{T} - 2T_\sigma] \quad (6)$$

where H is the thickness of the lower atmosphere. The parameters \bar{T} and T_σ are the mean and first moment of the temperature profile

$$\bar{T} = \frac{1}{H} \int_0^H T(z) dz \quad (7)$$

$$T_\sigma = \frac{1}{H^2} \int_0^H zT(z) dz. \quad (8)$$

In the case of a water vapor density profile, the vapor scale height (H_v) and integrated water vapor column are used to characterize the profile. Often water vapor density profiles are approximated by exponential function [17]

$$\rho_v = \frac{V}{H_v} \exp\left(-\frac{z}{H_v}\right) \quad (9)$$

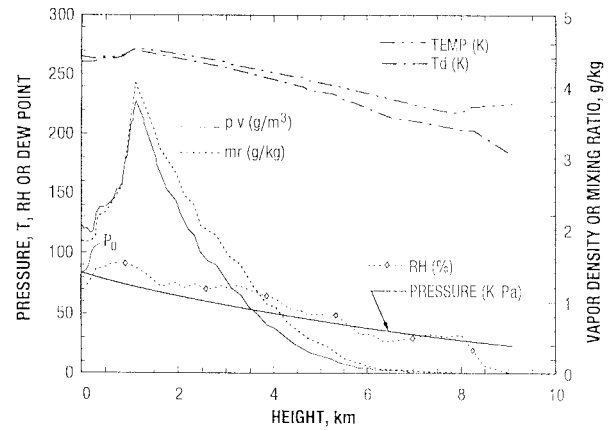


Fig. 1. Pressure, temperature, dew point, relative humidity, vapor density, and mixing ratio profiles measured by radiosonde at 15:00 GMT, 2 March 1991.

where V is integrated water vapor content

$$V = \int_0^H \rho_v dz \quad (10)$$

and

$$H_v = \frac{\int_0^H z\rho_v dz}{\int_0^H \rho_v dz}. \quad (11)$$

Although water vapor profiles measured by radiosondes rarely resemble exponential functions, vapor profiles can be approximated by (9) in the radiative transfer models of ground-based radiometers. The parameters V and H_v , which uniquely define (9), represent the information that can be extracted or retrieved from radiometer measurements. Some of the attempts to construct a water vapor profile using the integrated water vapor measurements by radiometers are not successful because the resulting profiles tend to be very smooth and lack detail [9].

Fig. 2 shows an example profile of an atmosphere. The water vapor density profile is defined by integrated water vapor content and its scale height (11). The linear temperature profile is defined by (4). Assuming two cloud layers, the first layer is an all-liquid homogeneous cloud, and its profile is specified by cloud base height (H_b), cloud thickness (D), and LWC. The second is an ice cloud and is placed above the liquid cloud layer; its profile is defined in a similar way as a liquid cloud except that the ice particle mean size (r_c) and bulk density (ρ) are also specified. The LWC and IWC in the two cloud layers are varied within their respective range of physical variations. The pressure profile, not plotted in Fig. 2, is derived from surface pressure and the temperature profile is constructed by vertical integration of hydrostatic equation [17]. To avoid unreasonable atmosphere structure, the following constraints are imposed: a) relative humidity must be less than or equal to 100% b) liquid cloud temperature be between -20 to 5 °C; c) ice cloud temperature must be below 0 °C, and d) the ice cloud base is above the liquid cloud top, consequently, co-existence of supercooled liquid water and ice particles is not allowed.

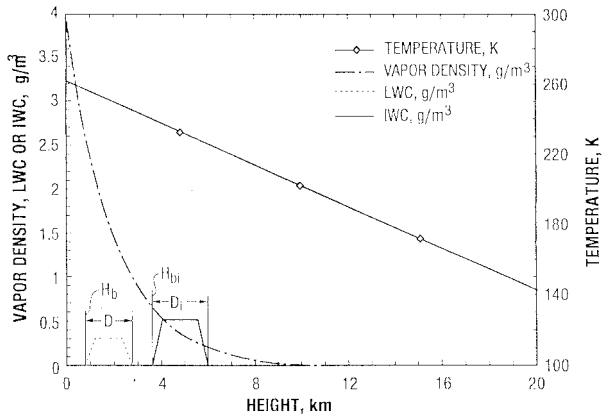


Fig. 2. An example of a parameterized atmosphere structure which is used as an input for the parametric radiative transfer model.

The above defined atmospheric profile is used to simulate brightness temperature data sets. In other words, radiosonde data are not needed for the simulation. Thus the construction of a retrieval algorithm is much more economical and faster, especially in a climatological area where radiosonde data are sparse. For example, each retrieval model developed in this paper was constructed in less than one week. It should be noted that meteorological parameters defined above form a complete set of input to our radiative transfer model. No other intermediate optical parameters are used; therefore, any intermediate retrieval algorithm is unnecessary.

IV. FORWARD MODEL

The radiative transfer process describes a nonlinear interaction between microwave emission, absorption, and scattering of atmospheric particles. In the atmosphere, microwave absorption and scattering are mainly due to molecular oxygen, water vapor, liquid water, and ice particles. Each of these components has different optical properties and absorption spectra. Water vapor absorption arises from a weak resonant line at 22.235 GHz, and a relatively strong continuum absorption term. For oxygen, there are two strong resonant lines around 60 and 118 GHz. Away from these two oxygen absorption lines, dry air absorption is very weak. We use Liebe's unified millimeter-wave propagation model (MPM) [18] to calculate the gaseous absorption. The MPM computes the microwave extinction coefficient of dry air and water vapor as a function of temperature, pressure, and humidity. In our model atmosphere, the water vapor profile is specified by vapor density as a function of height. To apply the MPM model, vapor density (ρ_v) is converted into a relative humidity profile (RH) using an empirical formula [18]

$$\text{RH} = \frac{e}{2.4089} \left(\frac{T}{300} \right)^5 \times 10^{(2950.2/T) - 10} \quad (12)$$

where T is the physical temperature, and e the partial water vapor pressure is given by the gas law

$$e = \rho_v R T \quad (13)$$

R is the gas constant for water vapor and is equal to $461 \text{ J deg}^{-1} \text{ Kg}^{-1}$ [17].

The MPM model computes emission properties of water vapor and oxygen at the frequencies of interest. These emission properties are combined with absorption and scattering characteristics of cloud droplets and ice in the subsequent radiative transfer model. It is important to quantify accurately the gaseous absorption component because the scattered downwelling radiation by an ice layer is modeled within a fraction of a Kelvin. In liquid cloud, absorption dominates over scattering. The Rayleigh approximation is applied to compute the absorption coefficients of cloud droplet ensembles. The Rayleigh absorption limit is valid for effective size $|n|k_0a \ll 1$, where n is the refractive index of liquid water, k_0 the free space wave number, and a the radius of water droplets. In the Rayleigh limit, the absorption coefficient is linearly proportional to liquid water content and is independent of drop size distribution [19]. Although the effective size (k_0a) of large liquid cloud droplets could exceed 0.2 or 0.3 at higher frequencies, the Rayleigh approximation is valid up to frequencies near 100 GHz due to the smallness of cloud droplets. The absorption of liquid water droplets increases with the decrease of physical temperature. Therefore, a liquid cloud with lower temperature looks brighter to the radiometers [12].

In an ice cloud, extinction is dominated by scattering and absorption is negligible. Ice particles are characterized by albedo close to unity with very little emission. The mean size of ice particles is on the order of sub-millimeters; ice crystals are usually nonspherical. Since we are interested in zenith-looking T_B observations, ice particle shapes are modeled by equivalent spheres and their scattering properties are calculated using the Mie scattering theory. A modified Gamma size distribution is used to average scattering properties of ice particle ensembles. Refractive indices of liquid water droplets and ice particles at the needed frequencies are obtained by interpolating the tabulated values in [20]. The invariant embedding method is applied to find the solution to the radiative transfer equation [19]. In the invariant embedding method, an arbitrary vertical structure is divided into a number of homogeneous layers. In each layer, the radiative transfer equation is rewritten in the form of interaction principle by making use of the finite-difference and Gaussian quadrature integral formula. To integrate properties of all infinitesimal layers, the linear nature of the interaction principle is used repeatedly. The formulation of radiative transfer in the form of the reflection and transmission matrices and emission source vectors of the whole medium also includes the boundary conditions of the transfer equations. In this way, the outgoing radiation and the radiation field inside the medium can be obtained from the interaction principle. We use land surface with an emissivity of 0.95, and let the ground temperature be equal to an effective near-surface temperature. At the top boundary, the cosmic radiation of 2.7 K is incident from above.

The theoretical description of absorption spectra of atmospheric constituents is incomplete. For example, the physical basis of absorption of water vapor continuum is not yet completely understood. Also, in the case of the liquid water absorption, we found that Liebe's MPM model differs from the Rayleigh approximation by about 1–6%. These discrepancies introduce biases into the radiative transfer model results.

Hence, a good calibration is essential to eliminate the inherent bias. One way to calibrate a physical model is to compare it with some well calibrated statistical algorithms, such as NOAA's ground-based dual-channel radiometer retrieval results. The calibration procedure is described in Part II of this paper.

V. PARAMETER MODEL TESTING AND SENSITIVITY STUDIES

To validate the performance of a parametric radiative transfer model, its results are compared against the rigorous radiative transfer method and radiometer measurements. The first test is based on radiosonde data plotted on Fig. 1. From sounding data, it is found that the integrated water vapor and vapor scale height are 0.85 cm and 1.82 km, respectively. The effective near ground temperature is 273.86° K and lapse rate is 5.986° K/km. For the purpose of model testing, cloud liquid and ice amount are assumed to be zero in this case. The results using rigorous radiative transfer model are 11.54, 10.67, and 28.95° K at 20.6, 31.65, and 90 GHz, respectively. These values are very close to the parameterized model simulation results, which are 11.36, 10.6, and 28.98 ° K.

In the second test, the observations made by the NOAA radiometer are used. NOAA ground-based dual-channel radiometers measure downwelling radiation in the zenith direction at 20.6 and 31.65 GHz. One of the facilities has an additional 90 GHz channel. The 20.6 GHz channel, which is offset from the weak water vapor resonant line at 22.235 GHz, senses mainly the integrated vapor and is less sensitive to the pressure and detailed structure of water vapor profiles. The 31.65 GHz is primarily sensitive to liquid water and the 90 GHz channel is in both absorption and scattering regime. On 2 March 1991, the NOAA radiometer measured 0.81 cm integrated water vapor and 0.018 mm liquid water. Cloud base height at 0.67 km was detected by a ceilometer; and the cloud top was estimated to be 0.85 km by the adiabatic approximation [10]. The corresponding measured brightness temperatures at the three channels are 16.04, 13.9, and 32.47° K. Using NOAA radiometer's retrieved vapor and liquid values, the corresponding parameterized model predicted brightness temperatures are 13.50, 11.8, and 32.24° K. The parameterized physical model results differ slightly from the actual observations and these differences are subsequently used to calibrate the neural network inversion models as explained in Part II of this paper.

Parameterized radiative transfer model not only simplified the process of solving radiative transfer equations but also preserved the main features of temperature and humidity profiles. The parameterized radiative model is initialized by 13 atmospheric components as listed in Table I. With a limited number of measurements from radiometers, it is difficult to invert this parametric model. Simulations might help to gain some insights into the dominant atmospheric components. But equally or more important is the sensitivities of brightness temperature T_B at a given channel to a particular atmospheric components (p_i), namely $\partial T_B / \partial p_i$ [16]. The basic idea of the sensitivity study is to cut the space along each dimension around a base state, and observe the behavior of the func-

tion along those cuts. A base state is primarily determined by mean-state of the above mentioned thirteen atmospheric components. In general, results of sensitivity studies are base state dependent. To describe an implicit function, three pieces of information are needed and they are its value, derivative, and dynamic range. Nonlinearity in the retrieval approach is identified by variation in sensitivities. The sensitivities are constant for linear retrieval algorithms. Nonlinearity in the model inversion is implemented with the aid of neural networks; the retrieval is problematic only if the sensitivities approach zero. For the development of an inverse model, it is also more important to identify insignificant parameters that are usually kept unchanged. Some of the insignificant parameters are treated as noise in both physical and statistical retrieval algorithms and they are not used in the model inversion procedure.

The sensitivity study was conducted at three frequency channels: 20.6, 32.65, and 90 GHz. A base state is chosen according to Denver winter time climate; namely $T_A = 0^\circ\text{C}$, $\Gamma = 6.5$ K/km, $V = 0.8$ cm, $H_v = 2$ km, $P_0 = 84$ kPa, $LWP = 200$ g/m², $D = 1$ km, $H_b = 1.5$ km, $IWP = 200$ g/m², $D_{ice} = 1$ km, $H_{bice} = 4.0$ km, $\rho = 0.92$ g/cm³, and $r_c = 0.05$ cm. The parametric model is examined in the neighborhood of this base state, which is referred as Base State 1.

Fig. 3 shows sensitivities of brightness temperature at each channel with respect to the integrated water vapor ($\partial T_B / \partial V$). In the range of interests, all three channels exhibit almost linear characteristics. Sensitivities are almost constant over the range of V , and they are 9.0, 4.2, and 16.0 K/cm at 20.6, 31.65, and 90 GHz channels, respectively. As expected, the 20.6 GHz channel is much less sensitive to integrated water vapor than 90 GHz channel, although 20.6 GHz is close to the water vapor resonance line at 22.235 GHz but it is more sensitive than the 31.65 GHz channel. Nevertheless, every channel shows certain sensitivity to integrated water vapor. As depicted in Fig. 4, the microwave brightness temperatures are much more sensitive to cloud liquid water than to vapor. Sensitivities at 20.6 and 31.65 GHz channels are almost constant. The 90 GHz response is in a nonlinear regime and its channel sensitivity drops quickly with the increase of the liquid water path. It is interesting to note that the 90 GHz channel will eventually saturate and loses its sensitivity to liquid water [6] in the absence of ice layer. At lower frequency such as the 31.65 GHz channel is still sensitive at these high LWP. Fig. 5 illustrates the brightness temperature sensitivity to the ice water path. The relationship is approximately linear over the range of interests. Ice cloud is optically thinner by at least a factor of two than liquid cloud around 90 GHz [23]. It is interesting to note that all three channels exhibit a sensitivity to ice path. An increase in ice water content by 1 g/m³ over 1 km path elevates the brightness temperature by about 5 K at 20.6 GHz, 14 K at 31.65 GHz, and 64.5 K at 90 GHz.

Brightness temperature is also very sensitive to bulk density and mean size of the ice particles as shown in Fig. 6(a) and (b). The sensitivity at 90 GHz increases rapidly with the increase of bulk density up to 0.7 g/cm³, and then it decreases until bulk density reaches its maximum value 0.92 g/cm³.

TABLE I
MODEL SENSITIVITY

Parameter(<i>p</i>)	Base State	$\frac{\partial T_{B20}}{\partial p}$	$\frac{\partial T_{B31}}{\partial p}$	$\frac{\partial T_{B90}}{\partial p}$	Unit	Sensitivity class
<i>V</i>	0.8 cm	7.0	4.2	16.3	K/cm	High
<i>LWP</i>	0.2 mm	31.0	62.5	199.0	K/mm	High
<i>IWP</i>	0.2 mm	5.0	14.0	64.5	K/mm	High
<i>P</i> ₀	84.0 KPa	0.06	0.13	0.27	K/KPa	Medium
ρ	0.92 g/cm ³	1.49	4.5	17.5	K cm ³ /g	Medium
<i>r</i> _c	0.05 cm	20.0	33.0	51.0	K/cm	Medium
<i>D</i>	1.0 km	0.6	1.0	0.2	K/km	Low
<i>D</i> _i	1.0 km	-0.05	-0.05	-0.15	K/km	Low
<i>H</i> _{bi}	4.0 km	-0.05	-0.05	-0.3	K/km	Low
Γ	6.5 °C/km	0.25	0.7	-0.2	K km/C	Low
<i>T</i> _A	0°C	-0.16	-0.3	0.2	K/C	Low
<i>H</i> _b	1.5 km	1.0	1.7	0.3	K/km	Low
<i>H</i> _v	2.0 km	-0.8	-0.6	-2.1	K/km	Low

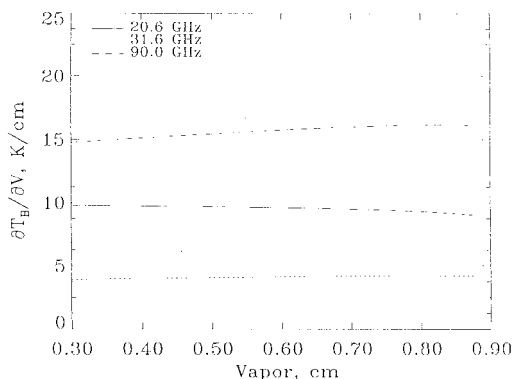


Fig. 3. Ground-based three-channel radiometer brightness temperature sensitivities to integrated water vapor ($\partial T_B/\partial V$) (*V*), as function of *V*.

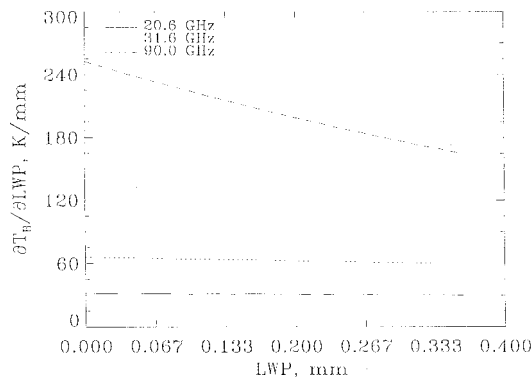


Fig. 4. Ground-based three-channel radiometer brightness temperature sensitivities to liquid water content (LWP) ($\partial T_B/\partial LWP$), as function of LWP.

However, the 90 GHz T_B values are more sensitive to LWP than to IWP. The sensitivity signatures in Fig. 6(a) and (b) indicate strong nonlinearity and can be explained as follows. The key to understanding these sensitivity signatures is that the IWP is constant in all our sensitivity calculations, except in cases where we studied sensitivity to IWP itself. Downwelling brightness temperatures increase with the optical depth of the ice layer. Increase in mode radius or number concentration will increase the optical depth. However, for a given IWP and bulk density, an increase in mode radius will result in decrease

of number concentration. As a result, the optical depth is a trade off between ice particle size and number concentration. As shown in Fig. 6(b), T_B sensitivity at 20 and 31 GHz channels increases first then decreases, but these sensitivities are always positive in the range of interests. This indicates that T_{B20} and T_{B31} increase with r_c in that range. For the 90 GHz channel, the sensitivity decreases monotonically from positive to negative. Hence, T_{B90} will increase initially and then decreases as r_c increases.

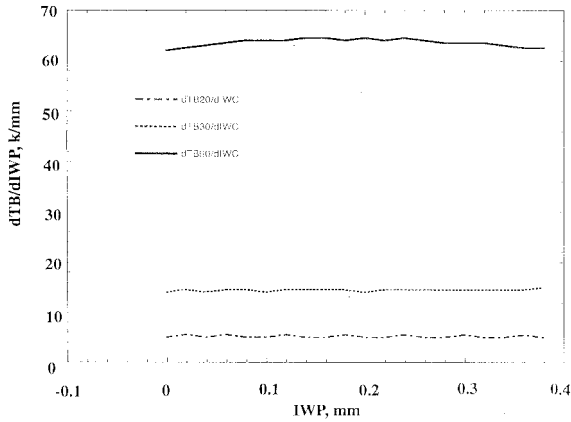
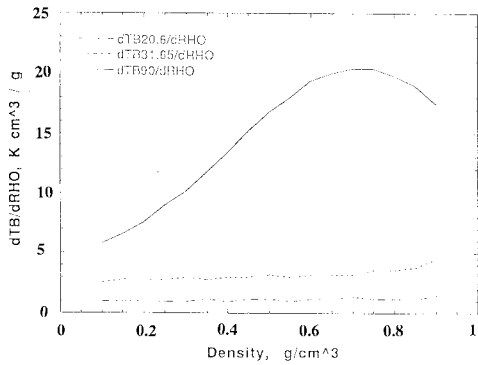
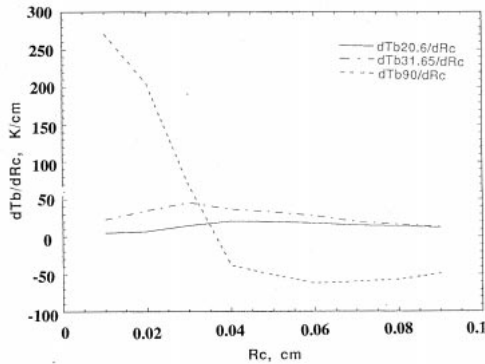


Fig. 5. Ground-based three-channel radiometer brightness temperature sensitivities to ice water content (IWP) ($\partial T_B/\partial \text{IWP}$), as function of IWP.



(a)



(b)

Fig. 6. Ground-based three-channel radiometer brightness temperature sensitivities to ice microphysics. (a) sensitivity with respect to bulk density ρ ($\partial T_B/\partial \rho$) as function of ρ ; (b) sensitivity with respect to mode radius ($\partial T_B/\partial r_c$) as function of r_c .

The impact of vapor scale height (H_v) on brightness temperature sensitivity is shown in Fig. 7. Changes in H_v affects both mean water vapor column temperature and vapor partial pressure which will in turn change the vapor mean radiation temperature, strength of vapor continuum absorption, and width of the absorption line at 22.2 GHz. As a net effect, the sensitivity decreases with H_v and becomes slightly negative for H_v greater than 1.5 Km. The 90 GHz channel shows the greatest sensitive to H_v , and 31.65 GHz is the least sensitive

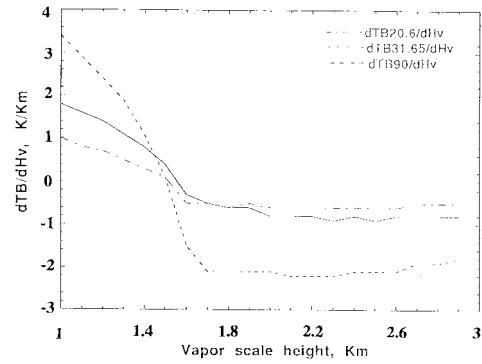


Fig. 7. Ground-based three-channel radiometer brightness temperature sensitivities to vapor scale height H_v ($\partial T_B/\partial H_v$) as function of H_v .

channel. But the sensitivity to H_v is relatively smaller than that due to LWP or IWP. Brightness temperature sensitivities to the rest of the model parameters, namely, H_b , T_A , Γ , D , and D_i are also studied. It is found that these parameters are less sensitive compared to that of V , LWP, IWP, ρ , and r_c .

The sensitivity of brightness temperature is quantitatively summarized in Table I. Thirteen model parameters are classified into three classes according to their sensitivities to brightness temperature, namely high, medium, and low. This kind of information or classification is very helpful when we construct physical retrieval models. In principle, sensitive parameters should be included in the retrieval algorithm; otherwise, they could introduce a large bias or pose strong limitations on the retrieval method. The procedure to incorporate all sensitive parameters into the inverse model is determined primarily by available measurements. If the number of measurements is larger than that of most sensitive physical parameters, it might be possible to include some of the slightly sensitive parameters and fix the rest of the variables at their meteorological mean values. For the insensitive variables, mean values should be used and their inclusion in the retrieval model will only complicate the algorithm.

The popular NOAA's linear statistical retrieval algorithm is based on long term radiosonde observation. A typical dual-channel algorithm for Denver area is given by [24] and [3]

$$V = -0.1705 + 0.10368T_{B20.6} - 0.04526T_{B31.65} \quad (14)$$

$$L = -0.0132 - 0.0008791T_{B20.6} + 0.002165T_{B31.65}. \quad (15)$$

The coefficients in the above equations change with climatological locations. It is interesting to compare the brightness temperature sensitivity derived from NOAA's inverse model and sensitivities computed using the parameterized radiative transfer model. Because the scattering due to ice cloud is ignored in NOAA's model, the sensitivity of physical model is calculated again around following Base State 2 $T_A = 273$ K, $\Gamma = 6.5$ K/km, $V = 0.5$ cm, $H_v = 2$ km, $P_0 = 84$ kPa, $D = 1$ km, $H_b = 1$ km. The ice water path is kept at zero, i.e. $\text{IWP} = 0.0$ g/m². The sensitivities from both models are compared in Figs. 8 and 9. The results show that the linear relationship between brightness temperature and integrated water vapor is a very good approximation.

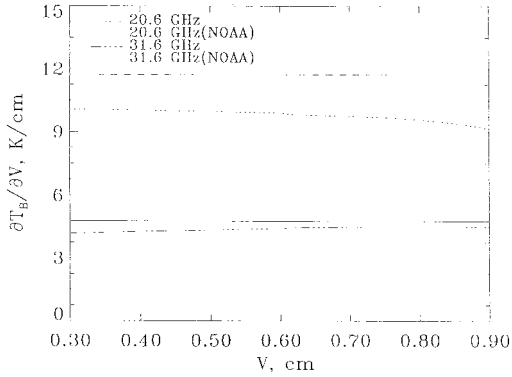


Fig. 8. Model sensitivity to water vapor path ($\partial T_B/\partial V$). Sensitivities between NOAA’s linear statistical inverse model and the parametric radiative transfer model are compared for the ground-based dual-channel radiometer.

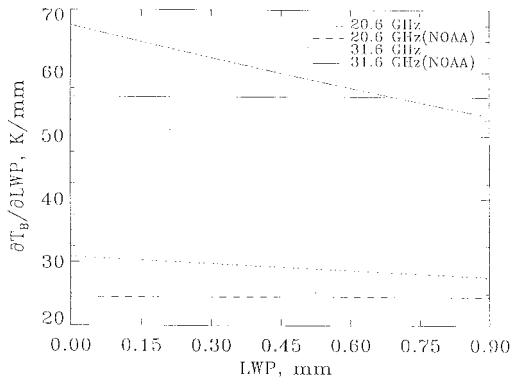


Fig. 9. Model sensitivity to liquid water path ($\partial T_B/\partial LWP$). Sensitivities between NOAA’s linear statistical inverse model and the parametric radiative transfer model are compared for the ground-based dual-channel radiometer.

The sensitivity differences between our model and NOAA’s linear statistical model is roughly estimated as shown in Table II(a). Base State 1 contains both ice and liquid clouds. In this case the parameterized model sensitivity deviates clearly from NOAA’s results. In principle, NOAA’s model should be accurate around the Base State 2 because their model is developed for ice free conditions.

In the absence of ice, the maximum difference between NOAA’s value and our physical model is 15%. The difference is small, especially when one considers the accuracy of the linear statistical model. Hogg *et al.* [3] compared the statistical model results and their corresponding radiosonde measurements taken at Denver in six months. They found that the rms difference between them is 1.7 mm for integrated water vapor. Wei *et al.* [25] did similar investigation on radiometer data collected at Shearwater, Nova Scotia, Canada. They assessed similar rms deviations for integrated water vapor and liquid water to be 0.867 mm and 0.159 mm, respectively, which are about 8.7% and 37% of the overall average vapor and liquid. The radiosonde itself is not a very accurate standard to compare with. Its performance is poor for relative humidity below 20% and above 90%, and reasonable otherwise [26].

We have analyzed sensitivities of the three-channel radiometer for a number of atmospheric parameters. Based on these

TABLE II
(a) SENSITIVITY COMPARISON UNIT: K/cm (b) THREE CHANNEL RADIOMETER SENSITIVITIES UNIT: K/cm

	$\frac{\partial T_{B20}}{\partial V}$	$\frac{\partial T_{B31}}{\partial V}$	$\frac{\partial T_{B90}}{\partial LWP}$	$\frac{\partial T_{B31}}{\partial LWP}$
NOAA Model	11.723	4.761	245.07	561.50
State 1	9.0	4.2	310	625
Difference (%)	23.0	12.3	-26.5	-11.3
State 2	10.038	4.23	273.06	517.40
Difference (%)	14.4	11.1	11.4	-7.85

(a)

	T_{B20}	T_{B31}	T_{B90}
Vapor	9.0	4.2	16.3
LWP	310	660	2000
IWP	50.0	140	645

(b)

studies, the most sensitive variables are identified and they are V , LWP, IWP and r_c . Since the primary objective is to retrieve V , LWP and IWP, sensitivities of these parameters for three channels are tabulated in Table II(b). The 20 GHz channel is affected by both vapor and liquid. Hence, NOAA’s dual-channel (20, 31 GHz) technique outperforms any single channel (20 GHz) method by retrieving vapor and liquid simultaneously. If we are interested in water vapor and liquid water retrievals in the absence of ice then, inclusion of the 90 GHz channel might not improve cloud liquid estimation. In the presence of IWP, the 30 GHz T_B is modulated by scattering ice layer. As expected the 90 GHz channel is sensitive to all of the three components, namely, V , LWP and IWP. The three-channel radiometer might be able to retrieve LWP with improved accuracy by taking into account ice layer scattering. Estimation of ice critically depends on precise estimations of V and LWP. Hence, both emission and scattering frequencies are necessary to retrieve ice information.

VI. NEURAL NETWORK MODELING

Recently, there has been increasing interest in using an artificial neural network to retrieve geophysical information from the passive microwave remote sensing measurements [27], [28]. Neural networks can handle nonlinearity in the remote sensing problems. It is also relatively easier for neural networks to incorporate auxiliary measurements and/or information into the retrieval algorithms. Here, we apply neural network techniques to the multiparametric retrieval from multifrequency T_B observations. We briefly discuss

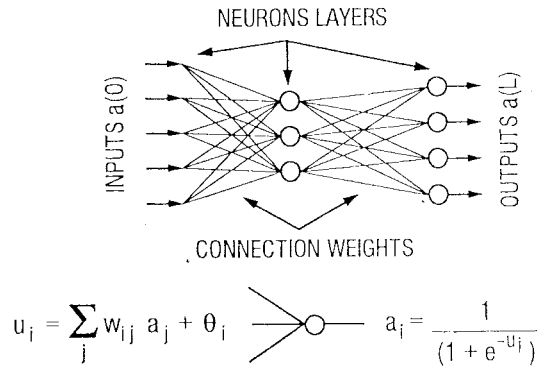


Fig. 10. The basic structure of a multilayer perceptron. The input layer feeds the input vector, multiplied by the associated connection weights, to the neurons of the next layer, where the multiplied input values are summed, added to an offset, and passed through a sigmoid function, the output of which serves as the input to the next layer of neurons.

one of the common neural network models, namely, the feedforward multilayer perceptron (MLP), then describe a procedure to construct data driven forward and inverse remote sensing models using MLP's.

A. Feedforward Multilayer Perceptrons

Fig. 10 illustrates the basic structure of a feed-forward MLP. The network can be described as a parameterized mapping from an input vector $a(0)$ to an output vector $a(L)$

$$\bar{a}(L) = \phi(\bar{W}, \bar{a}(0)) \quad (16)$$

where \bar{W} is the vector of weights, and L is the number of layers in the network. Passing a vector forward to the output layer consists of taking the inner product of the vector with the incoming weight vectors, and feeding the inner product into the nonlinear function of neurons. In the classical paradigm, training is the procedure of changing the weights to reduce the discrepancy between a target vector and the actual output vector $\bar{a}(L)$. The discrepancy, which is also called cost function (E), can take any form of a differentiable function. This offers us many ways to impose constraints and prior knowledge. Most often, this discrepancy is defined as sum squared error at the output units of the network, denoted by E

$$E = \frac{1}{2}(\bar{t} - \bar{a}(L))^T(\bar{t} - \bar{a}(L)) \quad (17)$$

where \bar{t} is the desired target vector and $\bar{a}(L)$ is the actual output vector. Backpropagation is an algorithm for computing the gradient of the cost function to minimize the cost. This is achieved by using the chain rule to differentiate the cost function (E) with respect to the weight vector W then updating the weights iteratively [29]

$$\bar{W}^{(n+1)} \leftarrow \bar{W}^{(n)} - \eta \frac{\partial E}{\partial \bar{W}^{(n)}} + \mu \Delta \bar{W}^{(n-1)} \quad (18)$$

$\bar{W}^{(n-1)} = \bar{W}^{(n)} - \Delta \bar{W}^{(n-1)}$, η and μ are learning rate and momentum parameter respectively. Once trained, an MLP can approximate an arbitrary input-output relationship [30].

B. Construction of a Forward and Inverse Model Using MLP

The general approach to solving inverse problems using MLP's is a two-phase procedure. In the first phase, a set of data generated from the parameterized radiative transfer model is used to train a data-driven neural network model that maps from parameter space (\bar{p}) to measurement space (\bar{m}). In other words, a causal relationship (ϕ) defined by the radiative transfer model $m = \phi(p)$ is copied by the neural network to obtain a forward model $\hat{m} = \hat{\phi}(p)$ as an approximation. It takes a meticulous effort to train the MLP; but once trained, a forward model can process the data speedily and accurately. More importantly, a forward model contains gradient information of measurements with respect to parameters. In the second phase, an inverse model is constructed based on this gradient information which provides us a way of searching for solutions in parameter space for a given measurement. This information may not be crucial when the inverse relationship is also causal.

In general, neural networks have little difficulty to learn forward problems since those mappings are unique. There are two important issues for a data driven forward neural network model (or forward model). One is how accurately the training and testing data set represent the situation being studied. This is a problem of sampling techniques. When the number of input units is too large, a favorite technique could be to create a grid of input variables and select points randomly in the grid. Otherwise, uniform sampling can be used. To evaluate a forward model, one can apply cross validation, training with one data set and testing with a different set, or test the model against independent synthetic data [28]. The second issue is how well the neural network can generalize or interpolate the training data. Since neural networks can approximate any function, their flexibility works against generalizations when the training data is noisy. For the problems studied in this paper, noise free training data is generated using our physical radiative transfer model. It is also found that a cross validation or a test against independent synthetic data is generally unnecessary.

One simple way to invert a neural network forward model is to train an inverse model by reversing the roles of the inputs and outputs. This method, known as explicit inversion, is widely used in remote sensing and in many other areas. Unfortunately, the radiative transfer model (or forward model) is characterized by many-to-one mapping. Although the mapping is uniquely determined by environment variables, inversion of such a forward model suffers one-to-many mapping. Explicit inverse method resolves such a mapping problem by averaging across the multiple targets. Specifically, if the cost function takes the form of sum-of-squared error, and one set of brightness temperature measurements corresponds to a number of environment states, the explicit inverse model will find an environment state which has minimum total Euclidean distance to all the corresponding environment states [28]. Furthermore, involved in the forward model are not only many-to-one functions, but also the geometry of the parameter space. As shown in Fig. 11, the inverse image of the forward model (nonlinear transformation) is not necessarily convex.

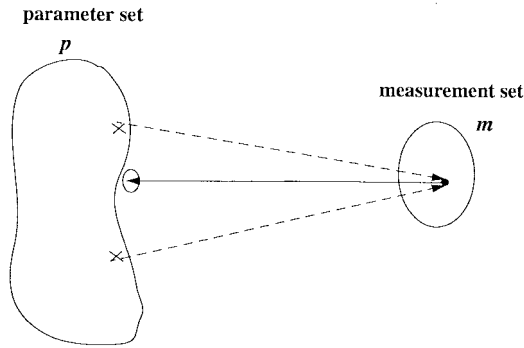


Fig. 11. The nonconvex problem. Forward model accurately maps each parameter to the resulting measurement set, while explicit inverses may face one-to-many mapping. The solid arrow line represents the direction in which the mapping is learned by explicit inversion. The two points lying inside the inverse image in parameter space are averaged by the learning procedure, yielding the vector represented by the small circle. This point is not a solution, because the inverse image is not convex.

The average point in a nonconvex set could be outside the set [31]. As a result, an average of many possible inversions may not be even an inversion. If one uses an explicit inverse model and retrieves certain atmospheric state for a given brightness temperature measurement, then feeds this retrieval into the forward model, the simulated brightness temperature could be different from the actual measurements. Therefore, the explicit inversion model is not usually consistent with the forward model. Iterative inversion algorithm to inverse a neural network is an interesting approach. The idea is to repeatedly present outputs to the forward model and search for a solution in the input space of the model while freezing the weights of the model. The algorithm is performed by computing the gradient of the cost functional with respect to the activation of the input units, and applying the iterative gradient decent algorithm to minimize the cost function E [28]

$$\bar{a}(0)^{(n+1)} \leftarrow \bar{a}(0)^{(n)} - (1 - \mu) \left(\eta \frac{\partial \bar{E}}{\partial \bar{a}(0)^{(n)}} / \left\| \frac{\partial \bar{E}}{\partial \bar{a}(0)^{(n)}} \right\| - \mu \Delta \bar{a}(0)^{(n-1)} \right). \quad (19)$$

In other words, instead of updating weights of networks, the iterative inversion approach updates inputs of forward models.

The iterative inversion and explicit inversion are fundamentally different. First, the iterative inversion approach finds a particular solution in the input (parameter) space, rather than an average over many possible solutions. The particular solution is one of the possible solutions, but the average solution obtained from explicit inversion may not be even be a solution. Second, the iterative approach starts with an initial guess. By choosing a initial guess properly, one can bias the trajectory movement to find the desired solution. In this way the iterative inversion is able to incorporate additional constraints or auxiliary information.

VII. RETRIEVAL USING NEURAL NETWORKS

In the earlier section, we described a methodology to construct neural network models for remote sensing applications.

The primary motivation is to make use of the inversion technique to retrieve V , LWP and IWP using three-channel radiometer observations. One of the critical issues in microwave remote sensing of atmosphere is to verify independently the quantities which have been retrieved. In spite of in-situ aircraft observations and radiosonde measurements, the independent quantification of atmospheric parameters such as LWP and IWP are incomplete. The incompleteness of in-situ observations limits the detail verification of neural network performance. In Part II of the paper, we compared the independent microwave radar and radiosonde observations with the neural network based radiometer retrievals. In this section, the performance of neural network models are evaluated by using a synthetic or simulated data set. This test is critical because the synthetic data are free of any system bias and noise. It should also be noted that synthetic data are limited by the assumptions in scattering and absorption models.

Based on sensitivity study results, we choose four model variables to build the parameter space: integrated water vapor (V), LWP, IWP, and surface pressure (P_0). The neural network outputs are three radiometer measurements: brightness temperatures T_B at 20.6, 31.65 and 90 GHz, and surface pressure P_0 . The rest of the model parameters are fixed at their mean state. Details are listed in Table III. It is to be noted that surface pressure is used as an auxiliary measurement and is included in both inputs and outputs of the network to assist the training. The training data set consists of 1920 data points generated with parametric radiative transfer model by sampling input space uniformly in the range of interest. As described earlier, both a forward and an explicit inverse model are trained. Each model has four input and output units, one hidden layer with 25 neurons. After 5000 batch training, the average output errors are 0.000 867 and 0.062 538 for the forward and explicit inversion models, respectively.

The next step is to evaluate the performances of explicit inversion and iterative inversion neural networks. For this purpose, a time series of vapor, liquid, ice and surface pressure are specified as in Fig. 12. Actual range of these quantities are specified in Table III and they are normalized between zero and unity for performance evaluation. The time series of vapor, liquid, ice, and pressure are completely independent of the training data set. These profiles are selected such that they represent a changing atmospheric condition and also ice and ice-free conditions. Using the radiative transfer model, the corresponding three-channel brightness temperatures are generated. These simulated T_B s are used in both explicit and iterative inversion models to retrieve the physical parameters shown in Fig. 12. The results of the explicit inversion model is given in Fig. 13. The retrieval accuracies for V and LWP are good. However, the retrieved IWP exhibits wild fluctuation. Between 0–10 h, the retrieved IWP values are greater than the original value by 0.03 mm. This might be a residual bias in the inversion model. The retrieval results using iterative inversion is displayed in Fig. 14. The inferred values are almost identical to the original ones. There is no significant bias in V , LWP or IWP values. Surface pressure is tracked very well. These results are far-superior to explicit inversion model values. Also we have constructed both two- and three-channel inversion

TABLE III
SCHEME 1

Retrieval variables	Range	Unit
V	(0.4, 0.97)	cm
LWP	(0.0, 800.0)	g/m^2
IWP	(0.0, 800.0)	g/m^2
P_0	(76.0, 86.0)	Kpa
Fixed Variables	Fixed value	Unit
ρ	0.5	g/cm^3
r_c	0.05	cm
H_b	1.5	Km
H_v	2.0	Km
T_A	-2.0	$^{\circ}C$
Γ	6.0	K/Km
H_{bi}	3.5	Km
D	1.0	Km
D_i	2.0	Km

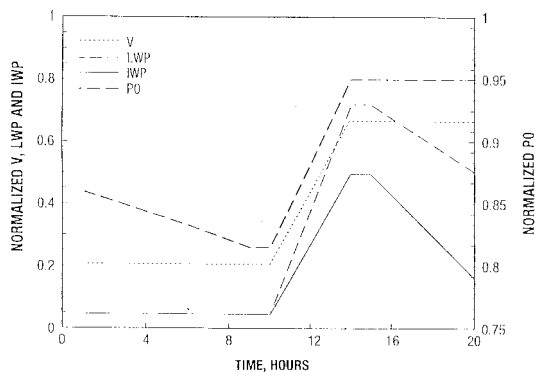


Fig. 12. Model atmospheric time series of normalized pressure, vapor, liquid, and ice components. This data set was used to simulate ground-based radiometer brightness temperatures using the parametric radiative transfer model.

models. The application of the neural network technique for a number of actual radiometer measurements are discussed in Part II of this paper.

VIII. CONCLUSIONS

We have developed a neural network-based inversion model to retrieve the columns of vapor, liquid, and ice. The tech-

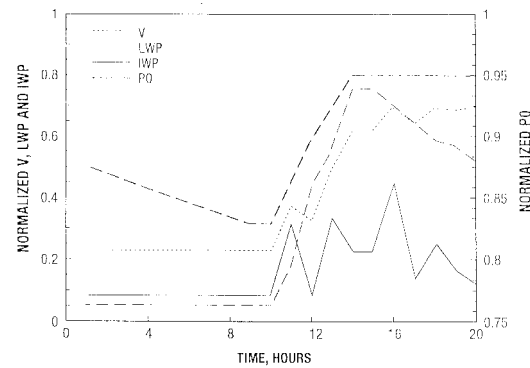


Fig. 13. Retrieved time series of normalized pressure, vapor, liquid, and ice components from simulated ground-based radiometer brightness temperatures using explicit inversion neural network modeling.

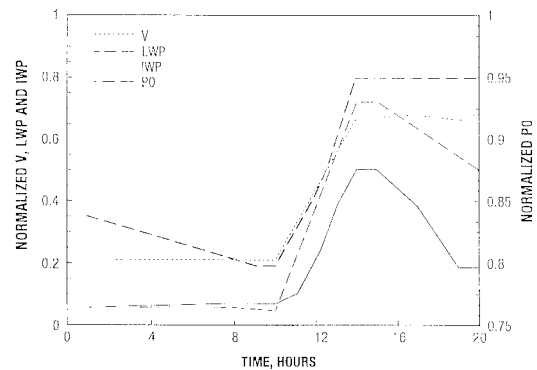


Fig. 14. Retrieved time series of normalized pressure, vapor, liquid, and ice components from simulated ground-based radiometer brightness temperatures using iterative inversion neural network modeling.

nique primarily uses ground-based two channel (20.6 and 31.65 GHz) and three-channel (20.6, 31.65 and 90 GHz) brightness temperatures. In the process of developing the inversion model, we performed detailed sensitivity studies of brightness temperatures with respect to more than thirteen different atmospheric quantities. Based on the sensitive studies, we demonstrated that 90 GHz T_B values are sensitive to IWP. Once the emission components such as vapor and liquid are accurately estimated, then enhancement in the 90 GHz T_B value are related to scattering due to ice layer. Precise quantification of vapor and liquid necessitated accurate parameterization of vertical profiles of temperature and vapor and also corresponding radiative properties of atmospheric gases. The MPM model is used to compute radiative properties of atmospheric gases. The resultant parameterized radiative transfer model includes emission and scattering to liquid and ice layer. Scattering due to ice is computed using Mie theory. The development of a parametric radiative transfer model with the detailed description of all of the atmospheric quantities is the key in the inverse model construction.

In practice, only a limited number of multifrequency brightness temperatures are available. Accordingly, we must narrow down the retrievable quantities and keep the rest of the parameters in a mean state. The above described methodology

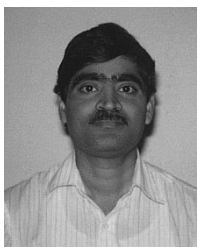
is feasible in a neural network approach. We constructed both explicit inversion and iterative inversion models. The explicit inversion model resolves the common syndrome of one-to-many mapping in the inversion process by averaging across the multiple solutions. On the other hand, the iterative inversion method freezes the weights of the neural networks and searches through the solution space by computing the gradient of the cost function with respect to the activation of input units and updates inputs of forward model. Also, this approach starts with an initial solution. Thus the iterative inversion finds a particular solution rather than an average over many possible solutions. The performance of both explicit inversion and iterative inversion are evaluated using a synthetic data set. This data set represented the dynamic nature of changing atmospheric conditions. The results demonstrated that the iterative inversion neural network model almost retrieved original input quantities. There is little bias or fluctuation in the results. The results are better than the standard explicit inversion model quantities. We have also constructed both two and three-channel inversion models. The applications of these techniques for a number of actual radiometer measurements are discussed in Part II of this paper. More importantly, the retrieved IWP is compared with radar estimates of the same.

ACKNOWLEDGMENT

The authors would like to thank Prof. J. N. Hwang of the University of Washington for developing the neural network models used in this research and NOAA's Environment Technology Laboratory which operates radiometer and K-band radar. The authors would also like to thank Dr. E. R. Westwater and J. Snider for contributing many useful ideas and providing the radiometer data, and Dr. R. Reinking and B. Kropfli for providing K-band radar data. J. Vivekanandan and L. Li would like to acknowledge Drs. R. Rasmussen and M. Politovich for useful discussions and M. Spencer for helping us with the quality controlled radiometer data.

REFERENCES

- [1] E. R. Westwater, "The accuracy of water vapor and cloud liquid determination by dual-frequency ground-based microwave radiometry," *Radio Sci.*, vol. 13, pp. 667–685, 1978.
- [2] F. O. Guiraud, J. Howard, and D. C. Hogg, "A dual-channel microwave radiometer for measurement of precipitable water vapor and liquid," *IEEE Trans. Geosci. Electron.*, vol. GRS17, pp. 129–136, 1979.
- [3] D. C. Hogg, F. O. Guiraud, J. B. Snider, M. T. Decker, and E. R. Westwater, "A steerable dual-channel microwave radiometer for measurement of water vapor and liquid in the troposphere," *J. Climate Appl. Meteor.*, vol. 22, pp. 789–806, 1983.
- [4] M. Blaskovic, B. E. Sheppard, R. R. Rogers, and T. C. Box, "Radiometric observations during the Canadian Atlantic Storms Program," *J. Atmos. Ocean. Technol.*, vol. 6, pp. 109–120, 1989.
- [5] D. H. Staelin, "Measurements and interpretation of the microwave spectrum of the terrestrial atmosphere near 1-centimeter wavelength," *J. Geophys. Res.*, vol. 71, pp. 2857–2881, 1966.
- [6] E. R. Westwater, "Ground-based microwave remote sensing of meteorological variables," *Atmospheric Remote Sensing by Microwave Radiometry*, M. A. Janssen, Ed. New York: Wiley, ch. 4, 1993.
- [7] E. R. Westwater and F. O. Guiraud, "Ground-based microwave radiometric retrieval of precipitable water vapor in the presence of clouds with high liquid content," *Radio Sci.*, vol. 15, pp. 947–957, 1980.
- [8] J. Askne and E. R. Westwater, "A review of ground-based remote sensing of temperature and moisture by passive microwave radiometry," *IEEE Trans. Geosci. Remote Sensing*, vol. GRS24, pp. 340–352, 1986.
- [9] S. F. Clifford, J. C. Kaimal, R. J. Latatits, and R.G. Strauch, "Ground-based remote profiling in atmospheric studies: An overview," *Proc. IEEE*, vol. 82, pp. 313–355, 1994.
- [10] B. B. Stankov, B. E. Martner, J. A. Schroeder, M. K. Politovich, and J. A. Cole, "Liquid water and water vapor profiling in multi-layered cloud using combined remote sensors," *31st Aerospace Science Meet. Exhibit*, Reno, NV, AIAA 93-0395, Jan. 11–14, 1993.
- [11] M. K. Politovich, B. B. Stankov, and B. E. Martner, "Use of combined remote sensors for determination of aircraft icing altitudes," *11th Int. Conf. Cloud and Precipitation*, Montreal, Canada, Aug. 17–21, 1992.
- [12] G. W. Petty and K. B. Katsaros, "The response of SSM/I to the marine environment. Part I—An analytic model for the atmospheric component of observed brightness temperatures," *J. Atmos. Oceanic Technol.*, vol. 9, pp. 746–761, 1992.
- [13] F. J. Wentz, "A model function for ocean microwave brightness temperatures," *J. Geophys. Res.* vol. 88, pp. 1892–1908, 1983.
- [14] M. K. Politovich, "Aircraft icing caused by large supercooled droplets," *J. Climate Appl. Meteor.*, vol. 28, no. 9, pp. 856–868, 1989.
- [15] D. Deirmendjian, *Electromagnetic Scattering on Spherical Polydispersions*. New York: Elsevier, 1969.
- [16] G. W. Petty, 1990: "On the response of the special sensor microwave/imager to the marine environment: Implications for atmospheric parameter retrievals," Ph.D dissertation, University of Washington, p. 291. [Available from University Microfilm, 305 N. Zeeb Rd., Ann Arbor, MI 48106].
- [17] P. V. Hobbs and J. M. Wallace, *Atmospheric Science: An Introductory Survey*. New York: Wiley, 1977.
- [18] H. J. Liebe, "MPM—An atmospheric millimeter-wave propagation model," *Int. J. Infrared Millimeter Waves*, vol. 10, pp. 631–650, 1989.
- [19] L. Tsang, J. A. Kong, and R. T. Shin, *Theory of Microwave Remote Sensing*. New York: Wiley, 1985.
- [20] P. S. Ray, "Broadband complex refractive indices of ice and water," *Appl. Optics*, vol. 11, p. 1836, 1972.
- [21] J. Vivekanandan, J. Turk, and V. N. Bringi, "Ice water path estimation and characterization using passive microwave radiometry," *J. Appl. Meteor.*, vol. 30, no. 10, pp. 1407–1421, 1991.
- [22] A. Mugnai and E. A. Smith, "Radiative transfer to space through a precipitating cloud at multiple microwave frequencies Part I: Model description," *J. Appl. Meteor.*, vol. 27, pp. 1055–1073, 1988.
- [23] P. Bauer and P. Schluessel, "Rainfall, total water, ice water, and water vapor over sea from polarized microwave simulations and special sensor microwave/imager data," *J. Geophys. Res.* vol. 98, no. 20, pp. 737–20,759, 1993.
- [24] G. E. Hill, "Measurement of atmospheric liquid water by a ground-based single-frequency microwave radiometer," *J. Atmos. Oceanic Technol.*, vol. 8, pp. 685–699, 1991.
- [25] C. H. Wei, G. Leighton, and R. R. Rogers, "A comparison of several radiometric methods of deducing path-integrated cloud liquid water," *J. Atmos. Oceanic Technol.*, vol. 6, pp. 1001–1012, 1989.
- [26] F. J. Schmidlin, "Radiosonde measurements: How accurate are they? How accurate must they be?" in *Proc. 8th Symp. Meteorological Observations Instrumentation*, 1993, pp. 93–97.
- [27] L. Tsang, Z. Chen, Seho Oh, R. J. Marks II, and A. T. C. Chang, "Inversion of snow parameters from passive microwave remote sensing measurements by a neural network trained with a multiple scattering model," *IEEE Trans. Geosci. Remote Sensing*, vol. 30, pp. 1015–1024, Sept. 1992.
- [28] D. T. Davis, Z. Chen, L. Tsang, J. H. Hwang, and A. T. C. Chang, "Retrieval of snow parameters by iterative inversion of a neural network," *IEEE Trans. Geosci. Remote Sensing*, vol. 31, pp. 842–852, July 1993.
- [29] D. E. Rumelhart, G. E. Hinton, and R. J. Williams, "Learning internal representations by error propagation," *Parallel Distributed Processing (PDP): Exploration in Microstructure of Cognition*. Cambridge, MA: M.I.T. Press, ch. 8, vol. 1, pp. 318–361, 1986.
- [30] K. Hornik, "Multilayer feedforward networks are universal approximators," *Neural Networks*, vol. 2, no. 5, pp. 359–366, 1989.
- [31] M. I. Jordan, D. E. Rumelhart, and E. David, "Supervised learning with a distal teacher," *Cognitive Science*, vol. 16, no. 3, pp. 307–354, 1992.



J. Vivekanandan received the B.E. degree in electronics and communications engineering from Madurai-Kamaraj University, the M.Tech. degree in microwave and radar engineering from the Indian Institute of Technology, Kharagpur, India, and the Ph.D. degree in electrical engineering from Colorado State University, Ft. Collins, USA.

At present he is a Scientist at the National Center for Atmospheric Research, Boulder, Colorado. His research experience includes radar and satellite remote sensing of the atmosphere, vegetation, and soil. He has devoted considerable effort toward modeling polarimetric radar and multifrequency satellite observations in clouds and their interpretations. He has participated in a number of field programs which involved radar, aircraft, satellite, and ground-based measurements.

Leung Tsang, (S'73-M'75-SM'85-F'90) received the S.B., S.M., and Ph.D. degrees from Massachusetts Institute of Technology, Cambridge, in 1971, 1973, and 1976, respectively.

He has been a Professor of Electrical Engineering at the University of Washington since 1986. His current research interests are in remote sensing, waves in random media and rough surfaces, and optoelectronics.

Dr. Tsang is co-author of the book *Theory of Microwave Remote Sensing* (Wiley-Interscience, 1985). Since 1996, he has been the Editor of the IEEE TRANSACTIONS ON GEOSCIENCE AND REMOTE SENSING. He was the Technical program Chairman of the 1994 IEEE Antennas and Propagation Symposium. He was also the Technical Chairman of the 1995 Progress of Research in Electromagnetics Symposium. He is the General Chairman of IGARSS'98. He is a Fellow of the Optical Society of America.

C. H. Chan, photograph and biography not available at the time of publication.